Catalysis Letters
https://doi.org/10.1007/s10562-020-03308-7

A Highly Dispersed Copper Nanoparticles Catalyst with a Large Number of Weak Acid Centers for Efficiently Synthesizing the High Value-Added 3-Methylindole by Aniline and Biomass-Derived Glycerin

Pinghui Sun[1] · Shuyi Lin[1] · Huimei Guo[1] · Jianhui Su[1] · Lei Shi[1]

Received: 6 May 2020 / Accepted: 30 June 2020

Abstract

An excellent catalyst with a large number of weak acid centers and highly dispersed copper nanoparticles embedded in mesoporous SBA-15 carrier was successfully constructed for the purpose of efficient conversion of aniline with biomass-derived glycerin to the high value-added 3-methylindole, in which the catalyst of Cu/SBA-15 was modified with Al_2O_3, La_2O_3 and CoO in sequence. The modified carrier and the copper-based catalysts were studied by scanning electron microscopy and energy-dispersive X-ray (SEM–EDX) spectroscopy, nitrogen physical adsorption, ammonia temperature programmed desorption (NH_3-TPD), hydrogen temperature programmed reduction (H_2-TPR), powder X-ray diffraction (XRD), transmission electron microscopy (TEM), thermogravimetric and differential thermal analysis (TG–DTA) and inductively coupled plasma (ICP) emission spectroscopy. The research found that the Cu/CoO/La_2O_3/Al_2O_3/SBA-15 catalyst exhibited a very good catalytic performance with 3-methylindole yield up to 73.3% and selectivity reaching 86.4%. Besides, only a 3.9% yield decreased after the catalyst was circulated seven times. The characterizations revealed that Al_2O_3 could enhance the polarity of the carrier, thereby the interaction between the active component and the composite carrier was strengthened and the dispersion of copper was increased significantly. Adding La_2O_3 to Cu/SBA-15-Al_2O_3 could weaken the acidity and inhibit the formation of carbon deposits. CoO promoter could increase the number of weak acid centers, which was conducive to a good dispersion of active component and the high selectivity of 3-methylindole. Furthermore, the reaction pathway of gas-phase synthesis of 3-methylindole from glycerin and aniline on Cu/CoO/La_2O_3/Al_2O_3/SBA-15 was explored.

Electronic supplementary material The online version of this article (https://doi.org/10.1007/s10562-020-03308-7) contains supplementary material, which is available to authorized users.

✉ Lei Shi
shilei515dl@126.com

[1] College of Chemistry and Chemical Engineering, Liaoning Normal University, Dalian 116029, Liaoning, China

Published online: 13 July 2020

Graphic Abstract

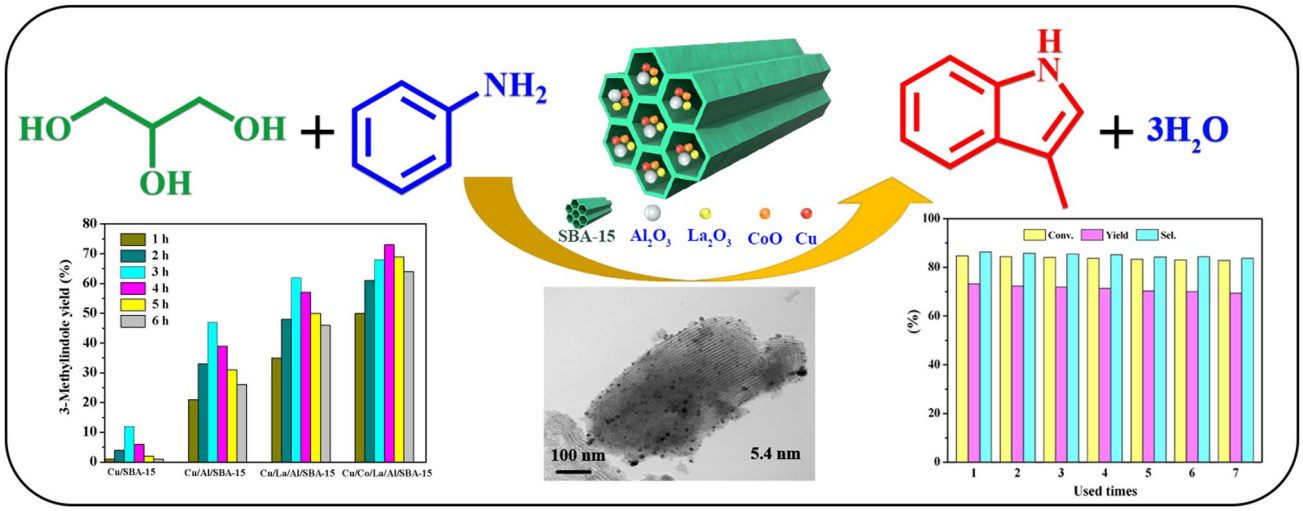

Keywords 3-Methylindole · Cu/SBA-15 · Al_2O_3 · La_2O_3 · CoO · Biomass-derived glycerin

1 Introduction

With the continuous development of economy and industrial production, the shortage of fossil fuels has become more and more serious. So the efficient use of renewable biomass resources to partially replace fossil fuels has received widespread attention [1–3]. Biodiesel, as one of the typical representatives of biofuels and a green energy source, has the advantages of renewable, degradable and low pollution, thereby the research about biodiesel production has attracted most of the attention in recent years [4, 5]. However, the production of biodiesel would emerge a large amount of by-product glycerin [6]. How to effectively convert glycerin to high value-added chemicals is a topic of great concern to chemical researchers [7–9], which can improve the sustainability and economic viability of biodiesel production. And by now, a lot of high value-added chemicals have been gained through various methods such as dehydration [8], hydrogenolysis [9], etherification [10], carboxylation [11], oxidation [12], transesterification [13], steam reforming of glycerin [6] and, etc. [14].

In our recent research, it was discovered that glycerin and aniline could be used to synthesize the high value-added chemical of 3-methylindole (3-MI), in which Cu/SiO_2-Al_2O_3 was the catalyst and a 40% 3-MI yield was obtained [15]. 3-MI is a crucial nitrogen-containing heterocyclic compound and has a wide range of application in industry, medicine and agriculture, such as used as a spices [16] and synthesizing dyes, feed additives, plant growth agents, pesticides, herbicides, fungicides and anti-inflammatory drugs, stimulants, antihypertensive drugs, vasodilator, anti-amine, anti-typhoid, anti-radiation and anti-cancer drugs, etc. [17, 18]. So important that 3-MI is, its synthesis methods, therefore, are widely concerned [19, 20].

Considering 3-MI synthesis methods, it can be known that gas-phase syntheses [21–24] and liquid-phase syntheses [25–27] are the most commonly used methods. For example, Campanati et al. [21] carried out the catalytic reaction with aniline and 1,2-propanediol as raw materials in a fixed bed at atmospheric pressure over ZrO_2/SiO_2, however, 3-MI yield was merely 12%. Our research group [22] used Ag/SiO_2 as a catalyst for the reaction, and the 3-MI yield increased to 35%. Gopal et al. [23] gained a 30% 3-MI yield over CeHZ zeolite catalyst using indole and methanol (1:6 molar ratio) as raw materials. Simoneau et al. [25] reported the Fischer cyclization of allylamine and 1-bromo-2-iodine-benzene catalyzed by Pd_2dba_3 with Nao–(tBu) and $PhCH_3$ as solvents, and a 85% yield of target product was obtained. For the liquid-phase syntheses, the 3-MI yield is relatively high, but some disadvantages exist such as complicated reagents, harsh reaction conditions, expensive catalysts and high cost of product separation [25–27]. Correspondingly, although the catalytic efficiency is not as good as that of the liquid-phase syntheses, the gas-phase syntheses have the advantages of environmental protection of raw materials, simple operation conditions and easy separation of products, etc. Thereinto, the gas-phase synthesis by using glycerin and aniline as raw materials is currently the most promising method and has attracted much attention because the reaction not only can convert the biomass-derived glycerin into the high

value-added chemical of 3-MI, which reduces the production cost of 3-MI remarkably, but also could promote the production of biodiesel [28].

According to the in-depth research of our research group, it has been found that Cu-based catalysts are active in this reaction. And in order to make the activity and selectivity of the catalyst as superior as possible, the catalyst carrier should have a high specific surface area and a large amount of weak acid centers [29–31].

The mesoporous SBA-15 is a good alternative as a carrier of heterogeneous catalyst because of its long-range ordered channels, high specific surface area, good hydrothermal stability and adjustable mesopore size [32–37]. And the unique hexagonal arrangement makes it be very suitable for supporting nano-scale metals [38, 39]. Therefore, in this paper, we select SBA-15 as the catalyst carrier to construct an efficient and inexpensive Cu-based catalyst. Considering the polarity of SBA-15 is very small, the interaction between SBA-15 and active components is very weak, which would make copper particles move and aggregate easily on the surface of the carrier, therefore, in this paper, the promoters of Al_2O_3, La_2O_3 and CoO were added to the catalyst of Cu/SBA-15 in order to improve the dispersion of the active component and increase the activity and selectivity of the catalyst. At the same time, SEM–EDX, N_2 physical adsorption, NH_3-TPD, H_2-TPR, XRD, TEM, TG–DTA and ICP characterization methods were used to explore the structure and performance of the catalysts. Furthermore, the synthesis mechanism of 3-MI by glycerin and aniline on Cu/CoO/La_2O_3/Al_2O_3/SBA-15 was studied profoundly and a reasonable pathway was proposed.

2 Experimental

2.1 Materials

Copper nitrate ($Cu(NO_3)_2{\cdot}3H_2O, \geq 99.0\%$), aluminium nitrate ($Al(NO_3)_3{\cdot}9H_2O, \geq 99.0\%$), lanthanum nitrate ($La(NO_3)_2{\cdot}6H_2O, \geq 99.0\%$), cobalt nitrate ($Co(NO_3)_3{\cdot}6H_2O, \geq 99.0\%$), aniline ($C_6H_5NH_2, \geq 99.5\%$), and n-hexanol ($C_6H_{13}OH, \geq 95.0\%$) were obtained from Tianjin Damao Chemical Reagent Co., Ltd. (China). Glycerin ($C_3H_8O_3, \geq 99.0\%$) was obtained from Zhaoqing Zhaolifang Trading Co., Ltd. Tetraethyl orthosilicate (TEOS, $(C_2H_5O)_4Si, \geq 98.0\%$), hydrochloric acid (HCl, 36% ~ 38%), acetol ($C_3H_6O_2, > 99.0\%$), 1,2-propanediol ($C_3H_8O_2, > 99.0\%$) and 3-MI ($C_9H_9N, > 98.0\%$) were obtained from Tianjin Kemiou Chemical Reagent Co., Ltd. (China). Pluronic P123 (Mn = 5800, $EO_{20}PO_{70}EO_{20}$) were obtained from Beijing Reagent Co., Ltd. (China). The above chemicals were not purified before use.

2.2 Preparation of SBA-15 Carrier and Copper-Based Catalysts

SBA-15 carrier was hydrothermally prepared based on the literature [40, 41] with a minor modification. A 4 g of P123 ($EO_{20}PO_{70}EO_{20}$) was dispersed in 160 mL (1.5 M) hydrochloric acid solution. After the solution was stirred thoroughly by the magnetic stirrer until the surfactant was wholly dissolved and uniformly dispersed, a 8.5 g TEOS was added into the above solution, and it was also stirred at 313 K for 24.0 h using a magnetic stirrer. Then the miscible liquid underwent an additional aging at 353 K for 24.0 h, and the suspension was filtered, washed. The sample was calcined in a muffle furnace at 773 K for 6.0 h after air-dried. Finally, the carrier of SBA-15 was obtained.

The catalyst of Cu/SBA-15 was obtained by equal volume impregnation method. At room temperature, take a certain amount of SBA-15 and immerse it in a suitable amount of copper nitrate aqueous solution. After 15.0 h of impregnation, dry it in a water bath of 368 K and next in an oven of 493 K for 4.0 h. Finally, place it in a muffle furnace, where it was calcined at the temperature of 773 K for 4.0 h. Then the catalyst precursor was prepared.

The catalyst of Cu/Al_2O_3/SBA-15 was acquired by sequential impregnation. The SBA-15 carrier was first soaked in a certain concentration of aqueous solution of $Al(NO_3)_3$ for 15.0 h. The mixture was then dried and calcined using the above method to obtain the modified carrier of Al_2O_3/SBA-15. Finally, the active component was loaded on the composite carrier of Al_2O_3/SBA-15 and the loading process was the same as the previous step.

The catalysts of Cu/La_2O_3/Al_2O_3/SBA-15 and Cu/CoO/La_2O_3/Al_2O_3/SBA-15 were also prepared by the same method as above and the loading sequence was Al_2O_3, La_2O_3, CoO in order, in which the active component was last loaded. For every SBA-15 supported copper-based catalyst, the loading of copper was 6.53 wt%. Before the catalytic reaction, the catalyst precursor (1.5 mL) was reduced at 513 K for 2.0 h with a mixture flow of H_2 (15 mL min^{-1})-N_2 (15 mL min^{-1}), which was the optimum reduction condition obtained by optimizing the reduction temperature, reduction time and reduction gas ratio.

2.3 Evaluation of Catalysts

The active measurement of catalyst was carried out in a glass reactor of fixed-bed with the inside diameter of 12 mm, which the reactor was placed vertically inside a tubular furnace and the temperature was monitored by a thermocouple with its tip located at the catalyst bed and connected to a temperature indicator controller. The reactant solution with glycerin/aniline molar ratio of 1:3 was pumped and vaporized by the preheater and then entered the reactor,

meanwhile a certain flow rate of hydrogen, nitrogen or steam was also introduced into the reaction system. The liquid products were hourly collected from the reactor exit. The space velocity (SV) of the reaction was 1700 h^{-1}, and the liquid hourly space velocity (LHSV) of aniline and glycerin was 0.4 h^{-1}.

2.4 Analysis of Products

In this paper, the products for the reaction of glycerin and aniline were qualitatively detected by using a QP2010 GC–MS instrument (Shimadzu Corporation, Japan) with DB-5MS column, in which the temperature was changed from 373 to 533 K at a 15 K min^{-1} heating rate. The qualitative analysis of 3-MI was proceeded on a 500 superconducting NMR spectrometer of Bruker and the result was shown in Fig. S1.

The reaction products were quantitatively determined by gas chromatography with HP-5 capillary column and N-hexanol was the internal standard. The glycerin conversion, 3-MI yield or selectivity was calculated as follows.

Glycerin conversion:

$$Conv.(\%) = \frac{n_{glycerin(initial)} - n_{glycerin(final)}}{n_{glycerin(initial)}} \times 100\%$$

3-MI yield:

$$Yield(\%) = \frac{n_{3-MI}}{n_{glycerin(initial)}} \times 100\%$$

3-MI selectivity:

$$Sel.(\%) = \frac{Yield}{Conv.} \times 100\%$$

2.5 Characterization of Catalysts

The compositions and each element content of Cu/CoO/La_2O_3/Al_2O_3/SBA-15 were examined using field-emission scanning electron microscopy of Germany Carl zeiss Supra55 with energy-dispersive X-ray spectroscopy (EDS) of UK Oxford X-MaxN. The acceleration voltage was 15 kV.

The N2 adsorption–desorption measurements of SBA-15 or its loaded Cu-based catalysts were accomplished using a physical adsorption instrument of Micromeritics ASAP 2010, where the sample was evacuated under 10–5 mmHg to purify at 573 K for 3.0 h.

The NH_3-TPD measurement was proceeded in a 6 mm × 350 mm quartz tubular reactor. Under He (35 mL min^{-1}) gas flow, 150 mg catalyst to be tested was heated from 293 to 773 K at a 9.6 K min^{-1} ramp rate, and impurities were removed. Then, the sample was absorbed by NH_3 at 373 K for 1.0 h, and the physically adsorbed NH_3 was blown away in 3.0 h at the same temperature in the helium flow (35 mL min^{-1}). Finally, the sample was heated to 973 K at a 9.6 K min^{-1} speed in a 35 mL min^{-1} He flow and stayed at 973 K for 0.5 h, in which the desorption data for the chemisorbed ammonia was collected.

H2-TPR experimental device is the same as the NH3-TPD instrument. 100 mg catalyst precursor was filled and heated to 573 K in N2 (30 mL min^{-1}) flow and purged at the temperature for 1.0 h to remove surface moisture and impurities, then the temperature was lowered to 313 K. Finally the reduction was carried out in a mixed gas (30 mL min^{-1}) of H2-Ar (VH2/VAr of 1/9) from 313 to 873 K and maintained the final temperature for 0.5 h, in which the data of hydrogen consumption were collected.

The crystal structures of SBA-15 carrier and its supported copper-based catalysts were detected on the Rigaku Smartlab 9 instrument using Cu-Kα radiation. The scan rate was 5° min^{-1}. A 200 mA tube current and a 45 kV tube voltage were used.

Use a JEM-2000EX microscope to obtain the TEM images of the catalysts, where the sample was ground down and put into ethanol solvent to uniformly be dispersed by ultrasonic treatment. The solution was then coated on a porous carbon copper mesh, and the transmission image of the sample was measured at 50 kV acceleration voltage.

The carbon deposits analyses for the used catalysts were carried out on a 6300 Diamond TG–DTA thermogravimetric instrument of PerkinElmer. A 7 mg sample was taken and purged at 573 K in a N_2 flow (20 mL min^{-1}), then it was dropped to 333 K. In the end, the sample was heated in an air flow of 20 mL min^{-1} from 333 to 1073 K at a 10 K min^{-1} rate.

The amounts of Cu component of the fresh or used SBA-15 supported Cu-based catalysts were tested by a Perkin Elmer Optima 2100DV inductively coupled plasma (ICP) emission spectroscopy, in which the RF power was 1300 W and a nebulizer (sample) argon flow was 0.80 L/min.

2.6 Catalyst Regeneration

The deactivated catalyst sample of Cu/CoO/La_2O_3/Al_2O_3/SBA-15 was regenerated at 773 K for 4.0 h in the mixed gas flow with oxygen (3 mL min^{-1}) and nitrogen (57 mL min^{-1}) after it was slowly heated to 773 K at 1 K min^{-1}. Then the cyclic activity test was conducted for the obtained sample.

3 Results and Discussion

3.1 Catalytic Performance

As is known to all, Cu-based catalysts are beneficial to the gas-phase synthesis of 3-MI by glycerin and aniline [15,

30, 31]. In addition, SBA-15 exhibits excellent performance as a catalyst carrier [32, 33, 42]. Hence, we use SBA-15 supported Cu as the catalyst for this reaction, and added an appropriate amount of Al_2O_3, La_2O_3 and CoO promoters to make the catalyst performance more superior. For the reaction, except the target product of 3-MI, many by-products were also detected. Among them, N-methylaniline (N-MA), N-ethylaniline (N-EA), N-isopropylaniline (N-IPA), 2,5-dimethyl-1-phenyl-pyrrole (2,5-DMPP) and 2,3-dimethylindole (2,3-DMI) were the major by-products. In addition, there were other by-products with minor amounts such as ethylic acid, N-propylaniline, propylene glycol, indole, 3-ketoneindole, N-isopropylindole and *N*,*N*′-dimethyl-*N*,*N*′-diphenyl-1,2-ethanediamine, etc. The activity and selectivity for the catalysts of Al_2O_3, La_2O_3 and CoO modified Cu/SBA-15 were shown in Tables 1, 2 and 3.

First at all, glycerin conversion, the selectivity for 3-MI and the by-products changed greatly when Al_2O_3 promoter was added to Cu/SBA-15 (seen in Table 1). The glycerin conversion was proportional to the content of Al_2O_3 added. The selectivity of 3-MI presented an earlier increase and later decreased trend with the increase of Al_2O_3 content. For the generated by-products, the selectivity of N-MA, 2,5-DMPP or 2,3-DMI increased with the increase of Al_2O_3 content, while N-EA or N-IPA selectivity decreased. When the content of Al_2O_3 was 11.03 wt%, 3-MI selectivity reached the better. From Table 2 it can be known that as the content of La_2O_3 increased, glycerin conversion decreased little by little, and the target product selectivity also exhibited a trend of going up first and then declining. The selectivity change trend of the major by-products was opposite to that in Table 1. In Table 3, glycerin conversion, the selectivity

Table 1 Effect of Al_2O_3 content on the activity and selectivity of Cu/Al_2O_3/SBA-15 catalyst

Al_2O_3 content (wt%)	Glycerin conversion (%)	Product selectivity (%)						
		3-MI	N-MA	N-EA	N-IPA	2,5-DMPP	2,3-DMI	Others
0.00	42.8	27.6	6.8	8.4	9.8	3.8	0.6	43.0
7.90	80.2	42.8	7.4	7.6	9.0	4.5	1.7	27.0
9.49	84.4	43.9	8.0	6.9	8.2	5.2	2.8	25.0
11.03	86.9	45.2	8.6	6.3	7.5	5.9	3.9	22.6
12.51	89.3	40.4	9.2	5.8	6.9	6.7	5.1	25.9
13.95	91.4	36.1	9.9	5.3	6.3	7.5	6.3	28.6

Reaction conditions: 513 K, H_2 = 15 mL min^{-1}, N_2 = 25 mL min^{-1}. The third hour results

Table 2 Effect of La_2O_3 content on the activity and selectivity of Cu/La_2O_3/Al_2O_3/SBA-15 catalyst

La_2O_3 content (wt%)	Glycerin conversion (%)	Product selectivity (%)						
		3-MI	N-MA	N-EA	N-IPA	2,5-DMPP	2,3-DMI	Others
0.00	86.9	45.2	8.6	6.3	7.5	5.9	3.9	22.6
0.54	85.4	51.4	6.9	6.4	7.6	4.7	3.1	19.9
0.81	83.9	56.2	5.1	6.6	7.8	3.3	2.2	17.8
1.07	82.6	63.1	3.8	6.8	8.0	2.3	1.5	14.5
1.34	80.3	59.7	3.3	7.4	8.5	1.8	1.2	18.1
1.60	77.2	57.5	3.0	7.9	9.0	1.5	0.8	20.3

Reaction conditions: 513 K, H_2 = 15 mL min^{-1}, N_2 = 25 mL min^{-1}. Al_2O_3 content of 11.03 wt%. The third hour results

Table 3 Effect of CoO content on the activity and selectivity of Cu/CoO/La_2O_3/Al_2O_3/SBA-15 catalyst

CoO content (wt%)	Glycerin conversion (%)	Product selectivity (%)						
		3-MI	N-MA	N-EA	N-IPA	2,5-DMPP	2,3-DMI	Others
0.00	82.6	63.1	3.8	6.8	8.0	2.3	1.5	14.5
0.18	84.8	65.8	4.0	5.6	6.6	2.9	2.2	12.9
0.25	86.9	69.2	4.2	4.0	4.9	3.6	2.8	11.3
0.31	88.4	65.4	4.7	3.7	4.0	4.9	4.1	13.2
0.37	90.1	59.3	6.4	3.4	3.8	6.8	6.2	14.1

Reaction conditions: 513 K, H_2 = 15 mL min^{-1}, N_2 = 25 mL min^{-1}. Al_2O_3 content of 11.03 wt%, La_2O_3 content of 1.07 wt%. The fourth hour results

for 3-MI and the major by-products showed the same change trend as that in Table 1 with the increase of CoO content. The optimal contents for La_2O_3 and CoO were 1.07 wt% and 0.25 wt%, respectively. And at this time, the activity and selectivity of Cu/CoO/La_2O_3/Al_2O_3/SBA-15 catalyst were optimal, which 3-MI yield reached 60.1%.

Figure 1 shows the glycerin conversion (A) and 3-MI yield (B) versus time on stream over Cu/SBA-15 and the catalyst modified with Al_2O_3, La_2O_3 and CoO promoter (Al_2O_3 content: 11.03 wt%, La_2O_3 content: 1.07 wt%, CoO content: 0.25 wt%). Over Cu/SBA-15, the conversion of glycerin was low and as the reaction proceeded, it decreased guadually. After adding the promoter of Al_2O_3, La_2O_3 and CoO to Cu/SBA-15 in order, glycerin conversion increased as a whole and it showed a slight downward trend versus time on stream, but the falling range became smaller.

The 3-MI yield versus time on stream over Cu/SBA-15 and the catalyst modified with Al_2O_3 or La_2O_3 gave the same change trend, which the yield of target product showed an upward trend within 1 to 3 h of reaction, and then began to decline. Adding Al_2O_3 and La_2O_3 promoters increased the yield of 3-MI greatly. After adding CoO to Cu/La_2O_3/Al_2O_3/SBA-15, 3-MI yield increased further and the highest yield of 60.1% was obtained at the fourth hour. It can clearly be seen that the deactivation of Cu/La_2O_3/Al_2O_3/SBA-15 modified with CoO was effectively suppressed, revealing the stability of the catalyst was greatly improved.

3.2 Characterization of Catalysts

3.2.1 SEM–EDX

Figure 2 presents the SEM images of Cu/CoO/La_2O_3/Al_2O_3/SBA-15 with the optimal content of Al_2O_3, La_2O_3 or CoO promoter, the content of each element and Si, O, Al, Cu, La and Co element mappings. It can be seen that the distribution of each element was relatively uniform. And as expected, the elements of silicon and oxygen were the most abundant, followed by the elements of aluminium, copper and lanthanum. The amount of cobalt element was least because Co content was only 0.25 wt%.

3.2.2 *N_2 Physical Adsorption*

The N_2 adsorption–desorption isothermals and the pore size distribution curves of SBA-15 and four copper-based catalysts with the optimal content of Al_2O_3, La_2O_3 or CoO promoter were shown in Fig. 3. It can be found from Fig. 3a that all the five samples have the same typical IV isotherm, which was the representative feature of mesoporous material [43, 44]. In the relative pressure of 0.4–0.7, the four Cu-based catalysts had the H-1 hysteresis ring as well as SBA-15 did, suggesting that the feature pore channels of the SBA-15 carriers of the Cu-based catalysts were not damaged after loaded the active component and promoters. The hysteresis loops were deformed and migrated downward slightly, indicating that their mesoporous sizes and ranges had changed [45].

From Fig. 3b, two kinds of pore size distribution can be seen on SBA-15, one was micropore at 1.9 nm, the other was mesopore at 2.2 nm. When the active component

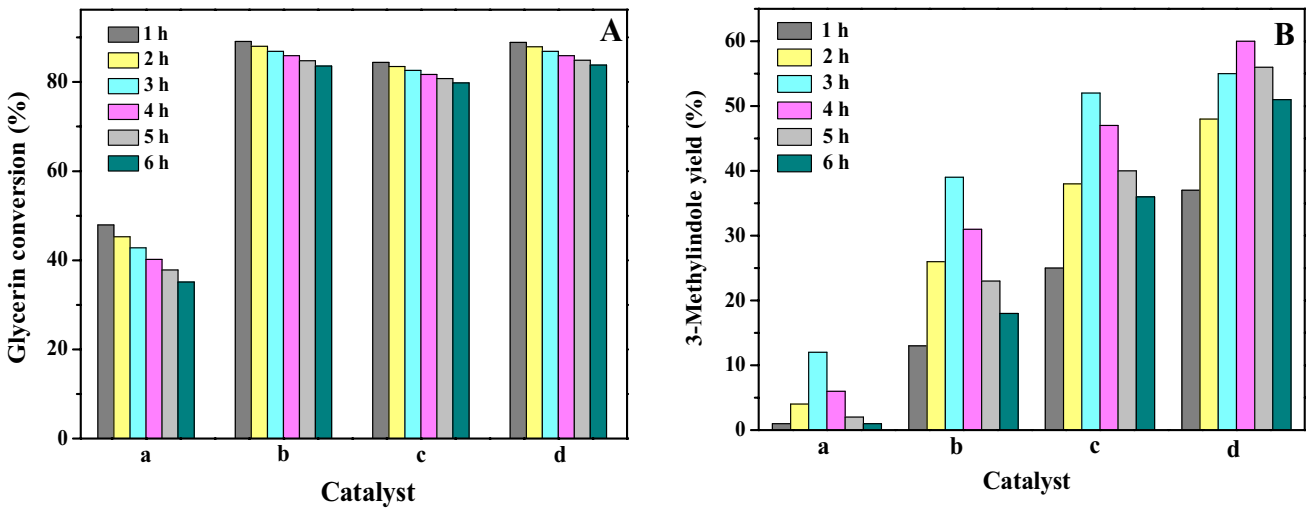

Fig. 1 The glycerin conversion (**A**) and 3-MI yield (**B**) versus time on stream over the catalysts of Cu/SBA-15 (*a*), Cu/Al_2O_3/SBA-15 (*b*), Cu/La_2O_3/Al_2O_3/SBA-15 (*c*) and Cu/CoO/La_2O_3/Al_2O_3/SBA-15(*d*)

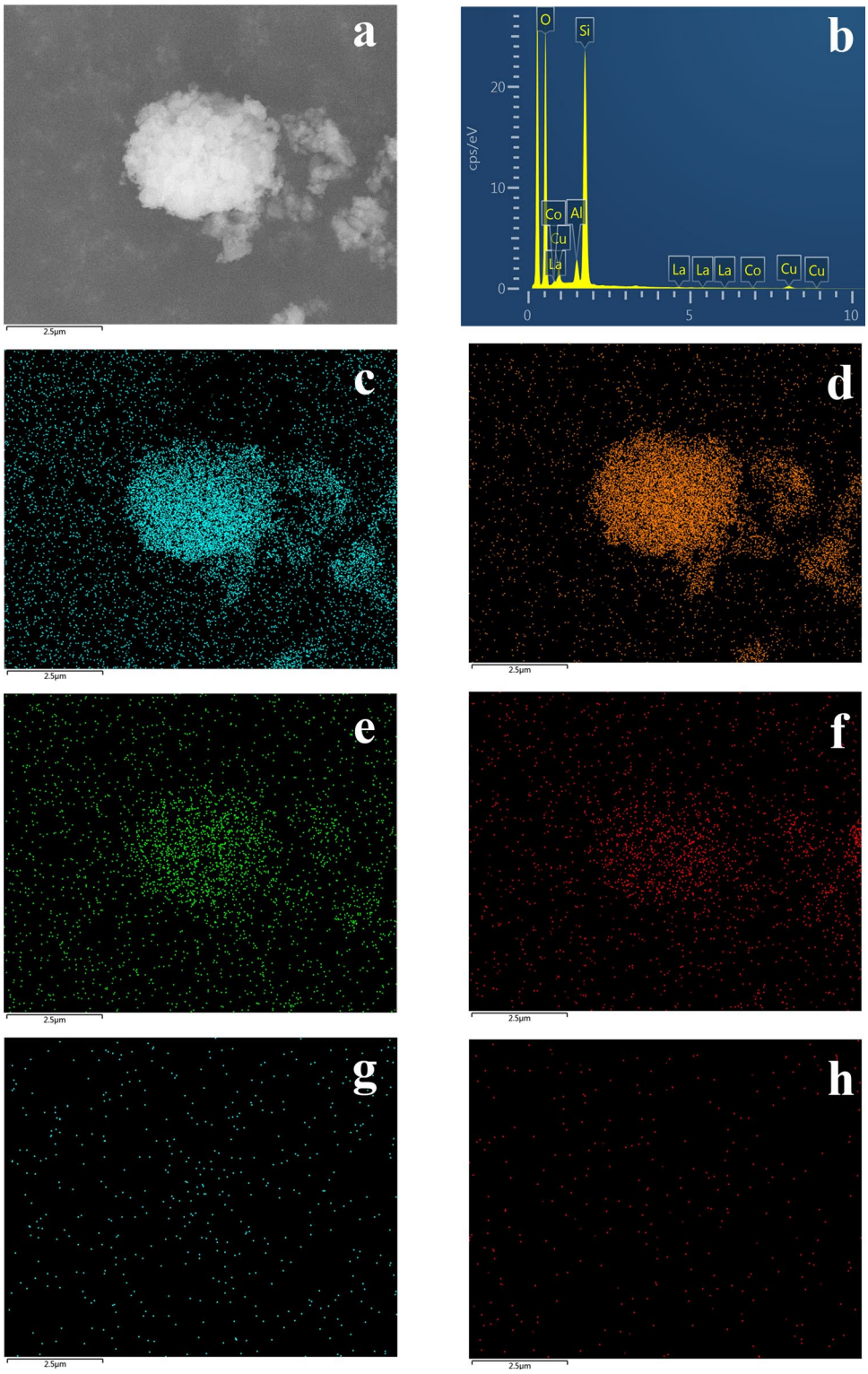

Fig. 2 SEM images (**a**), content of each element (**b**), elemental mappings of Si (**c**), O (**d**), Al (**e**), Cu (**f**), La (**g**) and Co (**h**) on Cu/CoO/La_2O_3/Al_2O_3/SBA-15 with Al_2O_3 content of 11.03 wt%, La_2O_3 content of 1.07 wt% and CoO content of 0.25 wt%

Cu was loaded on SBA-15, the amount of the mesopore increased, while the number of the micropore decreased. With the sequential addition of Al_2O_3, La_2O_3 and CoO promoters, the number of the micropore remarkably went down and the amount of the mesopore obviously augmented. This may be because a part of aluminum in the SBA-15 skeleton reacted with aluminum nitrate or cobalt nitrate with certain acidity, while a part of silicon in the SBA-15 skeleton reacted with lanthanum nitrate with

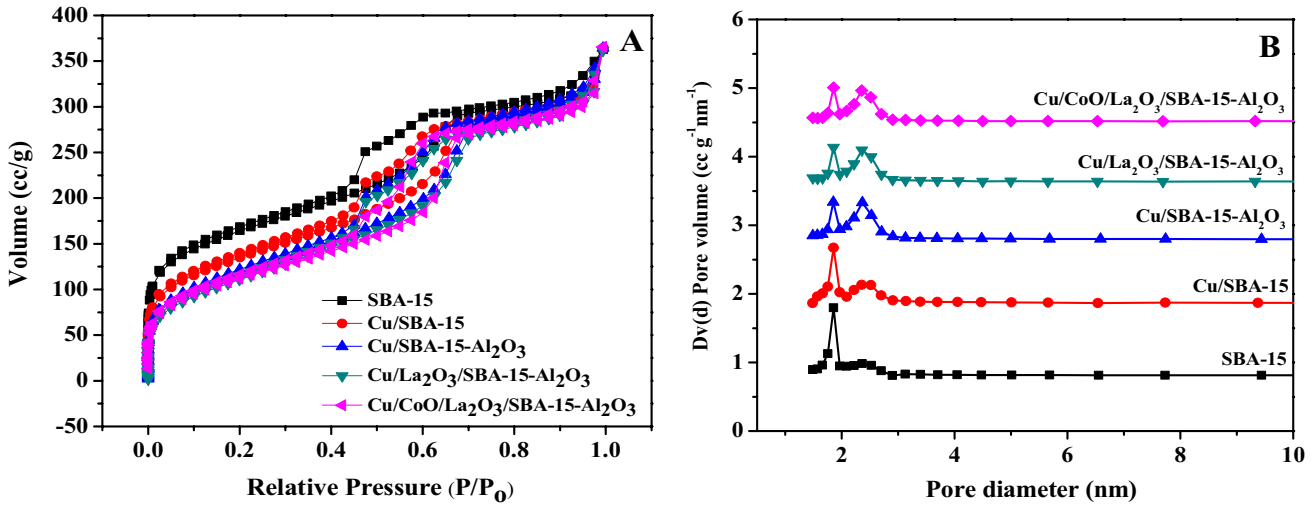

Fig. 3 N_2 adsorption–desorption isotherms (**a**) and the pore size distribution curves (**b**) of the samples of SBA-15, Cu/SBA-15, Cu/Al_2O_3/SBA-15, Cu/La_2O_3/Al_2O_3/SBA-15 and Cu/CoO/La_2O_3/Al_2O_3/SBA-15 with Al_2O_3 content of 11.03 wt%, La_2O_3 content of 1.07 wt% and CoO content of 0.25 wt%

certain basicity after immersing SBA-15 in the solution of aluminum nitrate, cobalt nitrate or lanthanum nitrate for a period of time (15 h), which resulted in the increase of pore size [46].

3.2.3 *NH_3-TPD*

The presence of acid centers is good for the adsorption of reactants of aniline and glycerin on the catalyst, but too strong acidity is not conducive to the desorption of 3-MI, which would cause a decrease in the yield and selectivity of 3-MI [30]. What's more, for the reaction of carbon-containing compounds, the strong acid centers will cause the formation of a large amount of carbon deposits, while the carbon deposits produced by weak acid centers are less. Therefore, this reaction requires a large number of weak acid centers. Figure 4 displays the NH_3-TPD profiles of Cu/SBA-15 and the modified catalysts with the optimal content of Al_2O_3, La_2O_3 and CoO. On Cu/SBA-15, only a broad desorption peak corresponding to medium-strong acid existed, no weak acid center appeared. After the promoter of Al_2O_3 was added into Cu/SBA-15, two large desorption peaks pertained to weak acid centers appeared, which was very beneficial to the high selectivity of target product [15, 31]. With the addition of La_2O_3, the acidity of the catalyst weakened and the number of weak acid centers declined, which could cut down the formation of carbon deposits. It's gratifying that the addition of CoO could also greatly increase the number of weak acid centers, which was beneficial to the further improvement for the selectivity of the target product.

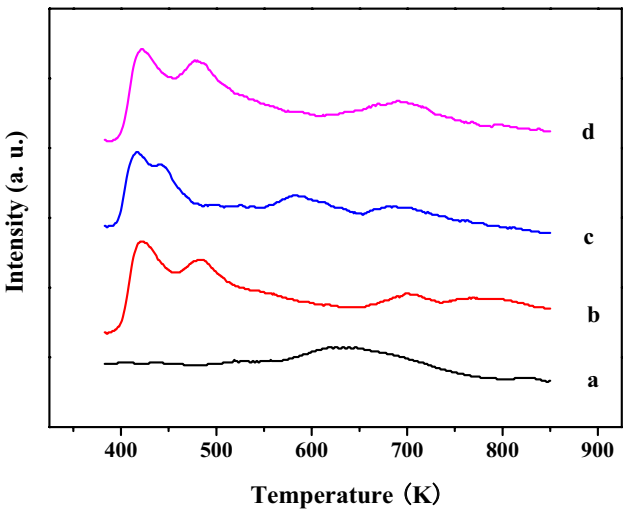

Fig. 4 NH_3-TPD profiles of Cu/SBA-15 (*a*), Cu/Al_2O_3/SBA-15 (*b*), Cu/La_2O_3/Al_2O_3/SBA-15 (*c*) Cu/CoO/La_2O_3/Al_2O_3/SBA-15 (*d*) with Al_2O_3 content of 11.03 wt%, La_2O_3 content of 1.07 wt% and CoO content of 0.25 wt%

3.2.4 *H_2-TPR*

The mutual effect between active component and carrier is one of many factors that affect the catalyst performance and H_2-TPR profile of the catalyst is a good proof to reveal the interaction. Figure 5 shows H_2-TPR profiles of CuO/SBA-15, CuO/Al_2O_3/SBA-15, CuO/La_2O_3/Al_2O_3/SBA-15, CuO/CoO/La_2O_3/Al_2O_3/SBA-15 and the composite carriers without CuO (Al_2O_3 content: 11.03 wt%, La_2O_3 content: 1.07 wt%, CoO content: 0.25 wt%). There was no reduction peak

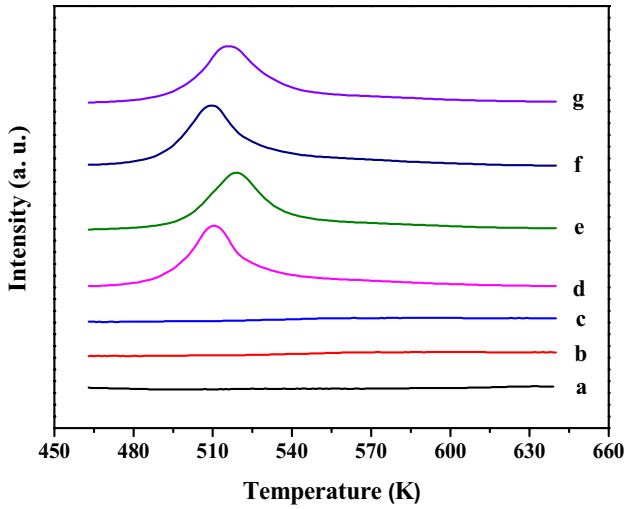

Fig. 5 H_2-TPR profiles of Al_2O_3/SBA-15 (*a*), La_2O_3/Al_2O_3/SBA-15 (*b*), CoO/Al_2O_3/SBA-15 (*c*), CuO/SBA-15 (*d*), CuO/Al_2O_3/SBA-15 (*e*), $CuO/La_2O_3/Al_2O_3$/SBA-15 (*f*), $CuO/CoO/La_2O_3/Al_2O_3$/SBA-15 (*g*) with Al_2O_3 content of 11.03 wt%, La_2O_3 content of 1.07 wt% and CoO content of 0.25 wt%

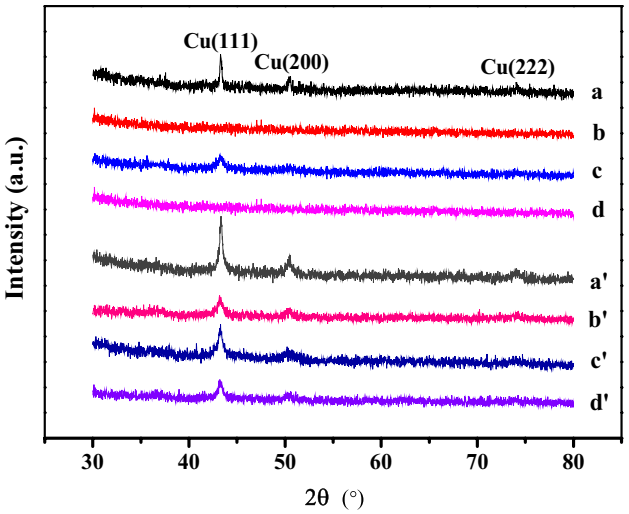

Fig. 6 XRD patterns of the fresh or used Cu/SBA-15 (*a*, *a′*), Cu/Al_2O_3/SBA-15 (*b*, *b′*), $Cu/La_2O_3/Al_2O_3$/SBA-15 (*c*,*c″*) $Cu/CoO/La_2O_3/Al_2O_3$/SBA-15 (*d*, *d′*) with Al_2O_3 content of 11.03 wt%, La_2O_3 content of 1.07 wt% and CoO content of 0.25 wt%

on the curve of a, b or c, only a reduction peak appeared on the curve of d, e, f or g, indicating that the reduction peak belonged to the reduction of CuO. CuO reduction peak shifted to the direction of high temperature after adding Al_2O_3, revealing that CuO was difficult to be reduced. This indicated that the promoter of Al_2O_3 could enhance the interaction force between CuO and the composite carrier. Adding the promoter of La_2O_3, however, brought about the reduction peak to shift to a low temperature, illustrating that the addition of La_2O_3 made CuO acquire electrons more easily and be reduced with easy. When CoO was added into $CuO/La_2O_3/Al_2O_3$/SBA-15, the reduction temperature of CuO increased from 509 to 517 K, meaning that the interaction between the carrier and CuO enhanced again. The above reduction phenomenon can be explained by the result of NH_3-TPD. Since the acidity of the catalyst raised after adding the promoter of Al_2O_3 or CoO, that is, the polarity of the catalyst molecule increased, which made the interaction force between CuO and the composite carrier enhanced, so CuO was difficult to be reduced. On the contrary, the acidity of the catalyst weakened after adding the promoter of La_2O_3, that is, the polarity of the catalyst molecule decreased, which brought about the force between CuO and the composite support weakened, therefore CuO was reduced easily.

3.2.5 XRD

In order to further explore the effect of Al_2O_3, La_2O_3 and CoO on the Cu dispersity, we performed the XRD measurement of the catalysts and Fig. 6 shows the patterns of the fresh and used copper-based catalysts. It can be observed that three typical diffraction peaks appeared at 2θ of 43.3, 50.5 and 74.5° on Cu/SBA-15 catalyst, pertained to the characteristic diffraction reflection of (111), (200) and (220) of copper crystal [47]. When Al_2O_3 promoter was added, the diffraction peaks of copper crystal had completely disappeared. This was due to the fact discussed in NH_3-TPD and H_2-TPR that the addition of promoter Al_2O_3 enhanced the force of copper and composite carrier, which hindered the aggregation of copper particles and made them be dispersed on the carrier. After adding La_2O_3 promoter to Cu/Al_2O_3/SBA-15, the intensity of the diffraction peak of copper increased a little, which can be explained from the fact that the interaction between Cu and the composite carrier reduced a bit as the addition of La_2O_3, so Cu particles aggregated slightly. The addition of CoO made the diffraction peak of Cu disappear again, illustrated the Cu particles were highly dispersed once more. The reason was naturally related to the increase of the force between Cu and the composite carrier.

Comparing the XRD patterns of fresh Cu-based catalysts, the intensity of the diffraction peaks of Cu crystal obviously enhanced on every used catalyst, which was attributed to the Cu sintering during the reaction. And on Cu/SBA-15, the sintering of Cu particles was most severe. Adding the promoter Al_2O_3 or CoO could significantly inhibit the sintering of Cu particles, while La_2O_3 promoter could not play the role. It was still due to the increase and decrease of the force of copper with the carrier after the addition of the three promoters.

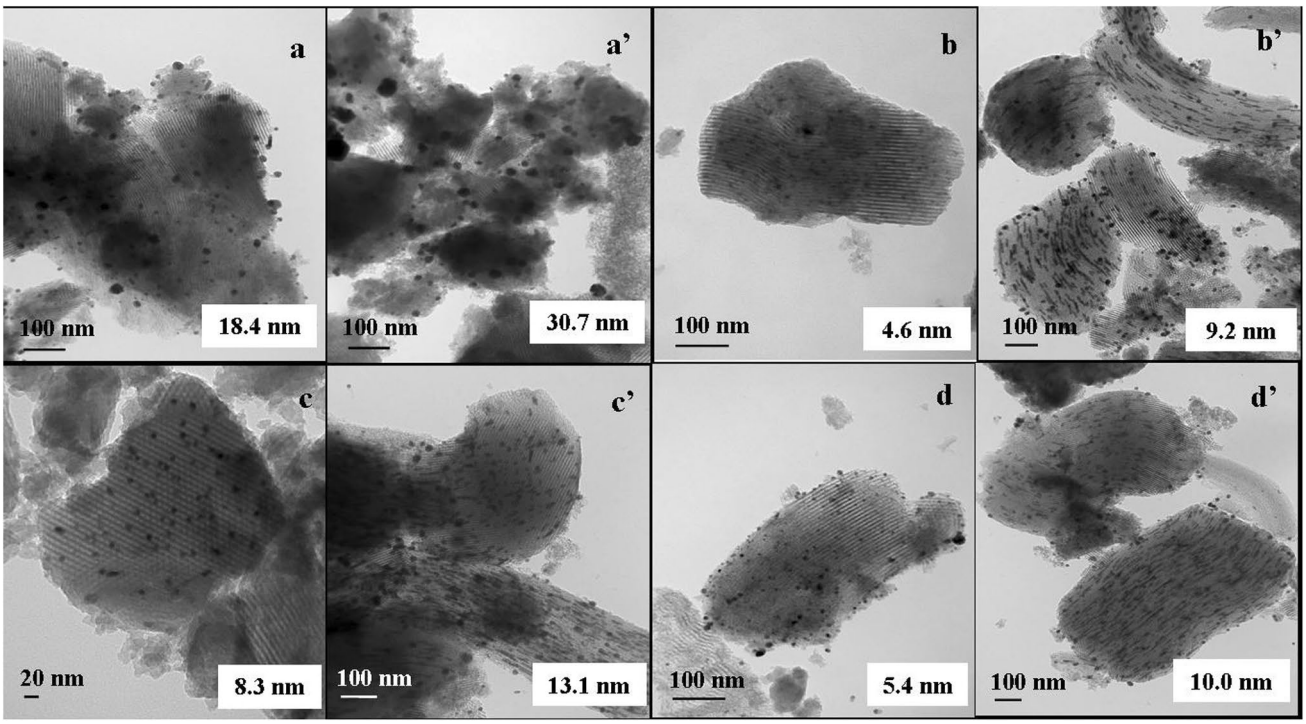

Fig. 7 TEM images of the fresh and used Cu/SBA-15 (*a*, *a*′), Cu/Al_2O_3/SBA-15 (*b*, *b*′), Cu/La_2O_3/Al_2O_3/SBA-15 (*c*, *c*′) and Cu/CoO/La_2O_3/Al_2O_3/SBA-15 (*d*, *d*′) with Al_2O_3 content of 11.03 wt%, La_2O_3 content of 1.07 wt% and CoO content of 0.25 wt%

3.2.6 TEM

For the sake of knowing the Cu particles size and the channel of SBA-15 carrier after loaded copper and three promoters on SBA-15 before and after the reaction, the TEM measurement (Fig. 7) of the fresh and the used Cu-based catalysts were proceeded (Al_2O_3 content: 11.03 wt%, La_2O_3 content: 1.07 wt%, CoO content: 0.25 wt%). The long-range uniform ordered strip channels can be observed after SBA-15 was loaded the active component Cu and three promoters. The Cu particles average diameter was 18.4 nm on the fresh Cu/SBA-15. The addition of Al_2O_3 reduced the average diameter of Cu particles to 4.8 nm, indicating that the promoter of Al_2O_3 improved the dispersion of Cu particles obviously. After adding La_2O_3 promoter to Cu/Al_2O_3/SBA-15, however, the average diameter of Cu particles augmented to 8.3 nm. After CoO promoter was doped to Cu/La_2O_3/Al_2O_3/SBA-15, the average diameter of Cu particles declined to 5.4 nm. The change of the average diameter of Cu particles is consistent with the aggregation of copper particles shown in XRD patterns.

From the image a′ it can be known that the average diameter of Cu particles on the used Cu/SBA-15 catalyst aggregated to 30.7 nm, illustrating that Cu particles were severely sintered. With the sequential addition of Al_2O_3, La_2O_3 and CoO promoters, the average diameters of Cu particles on the used catalysts were 9.2, 13.1 and 10.0 nm, respectively, manifesting that the sintering of Cu particles was effectively inhibited. Among them, Al_2O_3 and CoO played a very good role in improving the dispersion of Cu particles and inhibiting their sintering, which was also identified with the results of XRD. It's interesting, it can be seen in images b′, c′ and d′, a considerable part of the Cu particles were restricted in the SBA-15 strip-shaped channels, where they presented a channel streamline shape. So, it can be concluded that the composite SBA-15 carrier could limit the aggregation and sintering of active component to a certain extent.

3.2.7 TG–DTA

For the reaction with carbon compounds as raw materials, the acid centers will cause the formation of carbon deposits, which would reduce the catalyst activity until it is deactivated [48]. From the weight loss of the used Cu-based catalysts in Fig. 8, we can know the carbon deposits of the catalysts happened during the reaction. There was an obvious mass loss on Cu/SBA-15. After adding the promoter of Al_2O_3, the weight loss enhanced distinctly, revealed that Al_2O_3 facilitated the formation of carbon deposits. After adding La_2O_3 promoter to Cu/Al_2O_3/SBA-15, the weight loss decreased significantly. And the addition of CoO, however, increased the weightlessness again, indicating that CoO could not inhibit the formation of carbon deposits. The phenomenon was related to the acidity of catalyst. When Al_2O_3

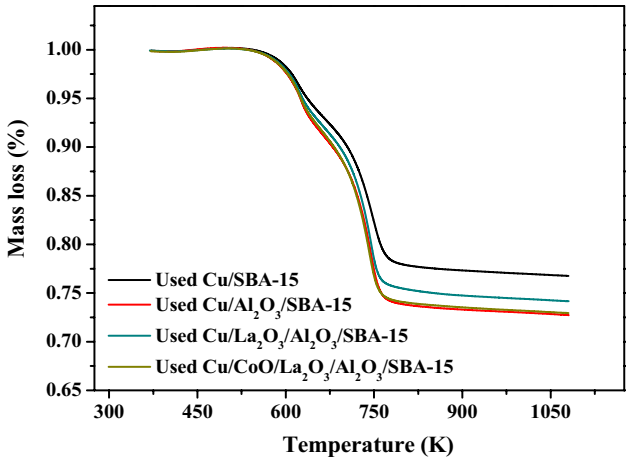

Fig. 8 TG results of the used catalysts of Cu/SBA-15, Cu/Al_2O_3/SBA-15, $Cu/La_2O_3/Al_2O_3$/SBA-15 and $Cu/CoO/La_2O_3/Al_2O_3$/SBA-15 with Al_2O_3 content of 11.03 wt%, La_2O_3 content of 1.07 wt% and CoO content of 0.25 wt%

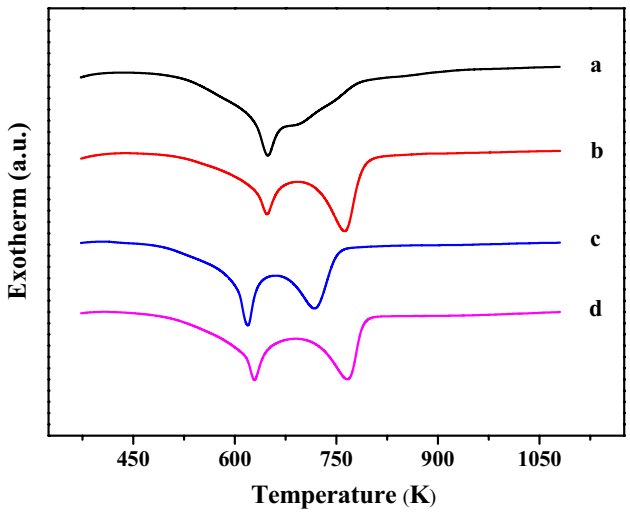

Fig. 9 DTA profiles of the used catalysts of Cu/SBA-15 (*a*), Cu/Al_2O_3/SBA-15 (*b*), $Cu/La_2O_3/Al_2O_3$/SBA-15 (*c*) and $Cu/CoO/La_2O_3/Al_2O_3$/SBA-15 (*d*) with Al_2O_3 content of 11.03 wt%, La_2O_3 content of 1.07 wt% and CoO content of 0.25 wt%

or CoO was added, the acidity of the catalyst increased, so more carbon deposits were formed. On the contrary, when La_2O_3 was added, the acidity of the catalyst was weakened, therefore the amount of the carbon deposition was less.

Figure 9 is DTA profiles of the Cu-based catalysts after 6 h of reaction. Obviously, after adding the promoter of Al_2O_3 to Cu/SBA-15, the type of carbon deposit of the catalyst changed. Although the exothermic peak at 647 K still existed, a new exothermic peak at 773 K appeared, and the area of this exothermic peak was much larger than that at 647 K, indicating that the amount of the carbon deposit

Table 4 Copper amount of the fresh or used SBA-15 supported Cu-based catalysts

Catalyst	Copper amount (wt%)	
	Fresh catalyst	Used catalyst
Cu/SBA-15	6.47	5.89
Cu/Al_2O_3/SBA-15	6.45	6.27
$Cu/La_2O_3/Al_2O_3$/SBA-15	6.51	6.22
$Cu/CoO/La_2O_3/Al_2O_3$/SBA-15	6.48	6.26

which was difficult to be oxidized was more. After adding La_2O_3 to the catalyst of Cu/Al_2O_3/SBA-15, both exothermic peaks moved towards the lower temperature, meaning that the carbon deposition type of the catalyst changed from the coke which was difficult to be oxidized at a higher temperature to the coke which was easy to be oxidized at a lower temperature. When CoO was added to $Cu/La_2O_3/Al_2O_3$/SBA-15, the exothermic peaks shifted to the high temperature again, demonstrating that the generated coke was more regular and more difficult to be oxidized.

3.2.8 ICP

Table 4 shows the copper amounts of the fresh or used SBA-15 supported copper-based catalysts (Al_2O_3 content: 11.03 wt%, La_2O_3 content: 1.07 wt%, CoO content: 0.25 wt%). 0.58, 0.18, 0.29 and 0.22 wt% loss of copper component were tested by ICP on Cu/SBA-15, Cu/Al_2O_3/SBA-15, $Cu/La_2O_3/Al_2O_3$/SBA-15 and $Cu/CoO/La_2O_3/Al_2O_3$/SBA-15 after 6 h of reaction. Obviously, the result was closely related to the effect of Al_2O_3, La_2O_3 or CoO promoter and it was in good agreement with the above discussion result.

3.3 Optimization of Reaction Conditions

The reaction conditions such as reaction temperature, hydrogen flow rate and steam flow rate were optimized over $Cu/CoO/La_2O_3/Al_2O_3$/SBA-15 (Al_2O_3 content: 11.03 wt%, La_2O_3 content: 1.07 wt%, CoO content: 0.25 wt%). From the data in Table 5, as the reaction temperature gradually augmented, the conversion of glycerin increased, the selectivity of 3-MI presented the trend of increasing first and decreasing. Among the by-products, N-MA, N-EA and N-IPA showed a downward trend, while 2,5-DMPP and 2,3-DMI exhibited an upward trend. When the reaction temperature was 523 K, the selectivity of target product achieved 71.9%. In Table 6, with the increase of hydrogen flow rate, the variation trend of glycerin conversion and 3-MI selectivity was the same as that in Table 5, while the selectivity change trend of the major by-products was opposite. When the flow rate of hydrogen was 10 mL

Table 5 Effect of reaction temperature on the activity and selectivity of Cu/CoO/La_2O_3/Al_2O_3/SBA-15

Reaction temperature (K)	Glycerin conversion (%)	Product selectivity (%)						
		3-MI	N-MA	N-EA	N-IPA	2,5-DMPP	2,3-DMI	Others
503	82.4	67.1	4.5	4.8	6.0	3.4	1.5	12.7
513	86.9	69.2	4.2	4.0	4.9	3.6	2.8	11.3
523	88.6	71.9	3.5	3.0	3.5	4.6	3.8	9.7
533	91.2	67.4	2.9	2.1	2.4	5.8	6.2	13.2

Reaction conditions: H_2 = 15 mL min^{-1}, N_2 = 25 mL min^{-1}. Al_2O_3 content of 11.03 wt%, La_2O_3 content of 1.07 wt% and CoO content of 0.25 wt%. The fourth hour results

Table 6 Effect of H_2 flow rate in reaction mixed gases on the activity and selectivity of Cu/CoO/La_2O_3/SBA-15-Al_2O_3 catalyst

$V_{(H2)}$ (mL min^{-1})	Glycerin conversion (%)	Product selectivity (%)						
		3-MI	N-MA	N-EA	N-IPA	2,5-DMPP	2,3-DMI	Others
5	86.1	73.3	2.6	2.4	2.4	5.5	3.2	10.6
10	87.9	77.1	3.1	2.7	3.0	5.0	3.5	5.6
15	88.6	71.9	3.5	3.0	3.5	4.6	3.8	9.7
20	91.2	67.4	3.8	3.4	3.9	4.3	4.2	13.0

Reaction conditions: 523 K, Al_2O_3 content of 11.03 wt%, La_2O_3 content of 1.07 wt% and CoO content of 0.25 wt%. The fourth hour results

Table 7 Effect of steam flow rate in reaction mixed gases on the activity and selectivity of Cu/CoO/La_2O_3/Al_2O_3/SBA-15 catalyst

V_{steam} (mL min^{-1})	Glycerin conversion (%)	Product selectivity (%)						
		3-MI	N-MA	N-EA	N-IPA	2,5-DMPP	2,3-DMI	Others
0	87.9	77.1	3.1	2.7	3.0	5.0	3.5	5.6
8	86.2	83.3	2.8	2.3	2.3	4.1	3.0	2.2
10	84.8	86.4	2.5	1.9	1.8	3.2	2.6	1.6
12	83.6	83.4	2.2	1.6	1.5	2.6	2.2	6.5

Reaction conditions: 523 K, H_2 = 10 mL min^{-1}, Al_2O_3 content of 11.03 wt%, La_2O_3 content of 1.07 wt% and CoO content of 0.25 wt%. The fourth hour results

min^{-1}, 3-MI selectivity reached 77.1%. Since an appropriate amount of steam is beneficial to removing carbon deposits generated during the reaction and improving the target product selectivity, the influence of the steam flow rate was explored. In Table 7, when the steam flow rate was 10 mL min^{-1}, 3-MI selectivity reached the top of 86.4% with the yield up to 73.3%. The excess steam resulted in a reduction for the target product selectivity because the chemical reaction equilibrium would shift to the direction of the reactants.

3.4 Reusability of Cu/CoO/La_2O_3/Al_2O_3/SBA-15 Catalyst

The reusability of Cu/CoO/La_2O_3/Al_2O_3/SBA-15 (Al_2O_3 content: 11.03 wt%, La_2O_3 content: 1.07 wt%, CoO content: 0.25 wt%) was tested. The catalyst underwent the regeneration after each run, and was reduced in situ again prior to activity test. Figure 10 shows the seven

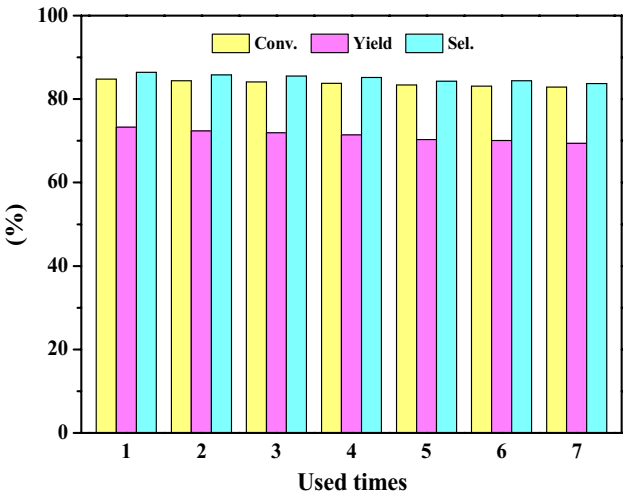

Fig. 10 Resuability study of Cu/CoO/La_2O_3/Al_2O_3/SBA-15 catalyst

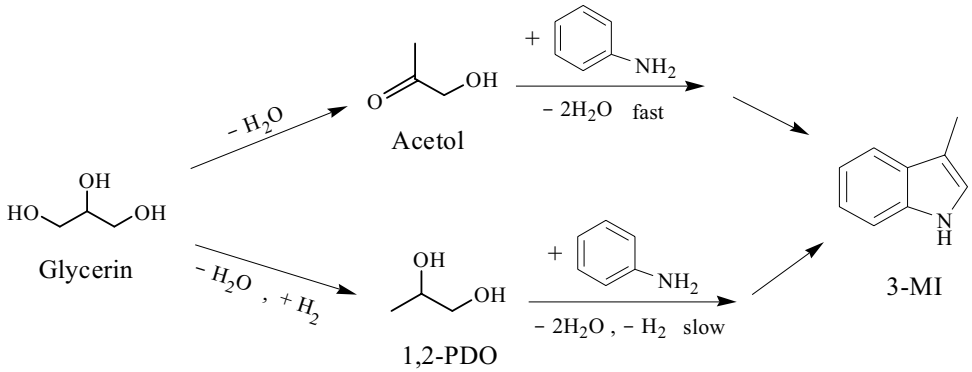

Scheme 1 Reaction pathway for the gas–solid synthesis of 3-MI by glycerin and aniline on Cu/CoO/La_2O_3/Al_2O_3/SBA-15

repeatability data about the fourth hour results of the reaction under the optimum reaction conditions over Cu/CoO/La_2O_3/Al_2O_3/SBA-15 catalyst. Only a 3.9% of 3-MI yield decreased when the catalyst was circulated seven times, indicating that it had a good practicality.

3.5 Reaction Pathway Research

To gain a clear idea of the reaction mechanism is what chemical researchers devote to do. In order to make clear the reaction pathway of the aniline with glycerin to 3-MI through gas-phase synthesis over the Cu/CoO/La_2O_3/Al_2O_3/SBA-15 catalyst, we did a series of investigations. First of all, we performed a GC–MS analysis to the reaction products. Except the target product of 3-MI, a 1.9% 1,2-propanediol (1,2-PDO) yield was also obtained. According to the relevant literature [49–52], glycerin can form 1,2-PDO through the hydrogenolysis over Cu-based catalysts. To test this, we have specifically done the hydrogenolysis of glycerin over the catalyst of Cu/CoO/La_2O_3/Al_2O_3/SBA-15. Only a 18.3% 1,2-PDO yield was obtained, while a large amount of acetol with the yield of 74.2% was detected. It has been reported [53, 54] that acetol could convert into 1,2-PDO, so the catalytic conversion of acetol was further proceeded on the catalyst, however, no 1,2-PDO was found. Since the related literature reported that 1,2-PDO can also be converted to 3-MI with aniline [55], the reaction of 1,2-PDO with aniline over Cu/CoO/La_2O_3/Al_2O_3/SBA-15 was carried out and the result confirmed this view. Moreover, in order to know whether the large amount of acetol produced in the hydrogenolysis of glycerin can be reacted with aniline to form 3-MI, we also carried out the reaction of acetol and aniline over the Cu/CoO/La_2O_3/Al_2O_3/SBA-15 catalyst. It was found that acetol was completely converted and a 80.6% 3-MI was produced.

Based on the above research, a possible pathway for the gas-phase synthesis of 3-MI by glycerin with aniline was proposed, as shown in Scheme 1. Acetol and 1,2-PDO were first produced through glycerin hydrogenolysis on the catalyst of Cu/CoO/La_2O_3/Al_2O_3/SBA-15. Then, acetol as well as 1,2-PDO reacted with aniline to generate the target product of 3-MI. Because the main product for the hydrogenolysis of glycerin was acetol and no acetol was tested in the reaction of glycerin with aniline, it can be deduced that the reaction of acetol with aniline was fast, while the conversion reaction of 1,2-PDO with aniline was slow.

4 Conclusion

3-MI was efficiently synthesized in a low-cost and green way over Cu/SBA-15 modified with Al_2O_3, La_2O_3 and CoO using biomass-derived glycerin and aniline as raw materials. During the reaction, the Cu/CoO/La_2O_3/Al_2O_3/SBA-15 catalyst exhibited predominant activity and selectivity. Through a series of characterization results it can be clearly known that the promoters of Al_2O_3 and CoO could enhance the acidity of the catalyst, thus the interaction force between Cu and the composite carrier increased, and thereby the Cu particles dispersity was higher and the sintering resistance was better. Moreover, the high selectivity of 3-MI benefited from a large number of weak acid centers after the addition of Al_2O_3 and CoO. The promoter of La_2O_3 weakened the acidity of the catalyst, which promoted the reduction of CuO and inhibited the formation of carbon deposits. Under the optimized reaction conditions with reaction temperature of 523 K and H_2 or steam flow rate of 10 mL min^{-1}, over Cu/CoO/La_2O_3/Al_2O_3/SBA-15 (Al_2O_3 content: 11.03 wt%, La_2O_3 content: 1.07 wt%, CoO content: 0.25 wt%), the optimum yield and selectivity of 3-MI were 73.3% and 86.4%, respectively. When the catalyst was reused 7 times, the yield of 3-MI still reached 69.4%, revealing the catalyst has excellent stability. Through the study on the reaction pathway it was concluded that glycerin could produce acetol and 1,2-PDO by hydrogenolysis on Cu/CoO/La_2O_3/Al_2O_3/SBA-15 catalyst. Acetol could fast react with aniline to form 3-MI. Although 1,2-PDO could also react with aniline to produce the target product, the rate was a little slow.

Acknowledgements We are gratefully thankful to the financial supported by the National Natural Science Foundation of China (Grant No. 21576128).

References

1. Wu HF, Liu QB, Bai Z, Xie XG, Zheng J (2019) Performance investigation of a novel multi-functional system for power, heating and hydrogen with solar energy and biomass. Energy Convers Manag 196:768–778. https://doi.org/10.1016/j.enconman.2019.06.040
2. Erdiwansyah MR, Sani MSM, Sudhakar K, Kadarohman A, Sardjono RE (2019) An overview of higher alcohol and biodiesel as alternative fuels in engines. Energy Rep 5:467–479. https://doi.org/10.1016/j.egyr.2019.04.009
3. Gielen D, Boshell F, Saygin D, Bazilian MD, Wagner N, Wagner R (2019) The role of renewable energy in the global energy transformation. Energy Strateg Rev 24:38–50. https://doi.org/10.1016/j.esr.2019.01.006
4. Adu-Mensah D, Mei D, Zuo L, Zhang Q, Wang J (2019) A review on partial hydrogenation of biodiesel and its influence on fuel properties. Fuel 251:660–668. https://doi.org/10.1016/j.fuel.2019.04.036
5. Gebremariam SN, Marchetti JM (2019) Economics of biodiesel production: review. Energy Convers Manag 168:74–84. https://doi.org/10.1016/j.enconman.2018.05.002
6. da SQ Menezes JP, Jácome FC, Manfro RL, Souza MM (2019) Effect of CaO addition on nickel catalysts supported on alumina for glycerol steam reforming. Catal Lett 149:1991–2003. https://doi.org/10.1007/s10562-019-02792-w
7. Tahir M, Siraj M, Tahir B, Umer M, Alias H, Othman N (2019) Au-NPs embedded Z-scheme WO_3/TiO_2 nanocomposite for plasmon-assisted photocatalytic glycerol-water reforming towards enhanced H_2 evolution. Appl Surf Sci. https://doi.org/10.1016/j.apsusc.2019.144344
8. Viswanadham B, Nagaraju N, Rohitha CN, Vishwanathan V, Chary KVR (2017) Synthesis, characterization and catalytic dehydration of glycerol to acrolein over phosphotungstic acid supported Y-Zeolite catalysts. Catal Lett 148(1):397–406. https://doi.org/10.1007/s10562-017-2236-9
9. Suthagar K, Shanthi K, Selvam P (2018) Hydrogenolysis of glycerol over silica-supported copper-nanocatalyst: effect of precipitating-agent and copper metal-loading. Mol Catal 458:307–316. https://doi.org/10.1016/j.mcat.2017.11.035
10. Bozkurt ÖD, Bağlar N, Çelebi S, Uzun A (2019) Assessment of acid strength in sodium-exchanged resin catalysts: consequences on glycerol etherification with isobutene in batch and flow reactors. Mol Catal 466:1–12. https://doi.org/10.1016/j.mcat.2018.12.027
11. Razali NA, Conte M, McGregor J (2019) The role of impurities in the La_2O_3 catalysed carboxylation of crude glycerol. Catal Lett 149:1403–1414. https://doi.org/10.1007/s10562-019-02679-w
12. Abis L, Dimitratos N, Sankar M, Freakley SJ, Hutchings GJ (2019) Plasmonic oxidation of glycerol using Au/TiO_2 catalysts prepared by sol-immobilisation. Catal Lett 150:49–55. https://doi.org/10.1007/s10562-019-02952-y
13. Parameswaram G, Rao PSN, Srivani A, Rao GN, Lingaiah N (2018) Magnesia-ceria mixed oxide catalysts for the selective transesterification of glycerol to glycerol carbonate. Mol Catal 451:135–142. https://doi.org/10.1016/j.mcat.2017.12.006
14. Hejna A, Kosmela P, Formela K, Piszczyk Ł, Haponiuk JT (2016) Potential applications of crude glycerol in polymer technology–current state and perspectives. Renew Sust Energ Rev 66:449–475. https://doi.org/10.1016/j.rser.2016.08.020
15. Sun W, Liu DY, Zhu HY, Shi L, Sun Q (2011) A new efficient approach to 3-methylindole: vapor-phase synthesis from aniline and glycerol over Cu-based catalyst. Catal Commun 12:147–150. https://doi.org/10.1016/j.catcom.2010.08.011
16. Yu XY, Xiu XH, Feng XC, Yan CL, Liu SF, Zheng LF, Liu ZJ (2018) Determination of indoles and 3-methylindoles in rat feces by HPLC in different environments. Chin J Mod Appl Pharm 11:1597–1601. https://doi.org/10.13748/j.cnki.issn1007-7693.2018.11.001
17. Wan YC, Li YH, Yan CX, Yan M, Tang ZL (2019) Indole: a privileged scaffold for the design of anti-cancer agents. Eur J Med Chem 183:111691. https://doi.org/10.1016/j.ejmech.2019.111691
18. Vargas DA, Méndez LJ, Cánepa AS, Bravo RD (2017) Sulfated zirconia: an efficient and reusable heterogeneous catalyst in the friedel–crafts acylation reaction of 3-methylindole. Catal Lett 147:1496–1502. https://doi.org/10.1007/s10562-017-2057-x
19. Hakim SSMA, Touchy AS, Jamil MdAR, Toyao T, Shimizuet K (2018) C-methylation of alcohols, ketones, and indoles with methanol using heterogeneous platinum catalysts. ACS Catal 8:3091–3103. https://doi.org/10.1021/acscatal.7b04442
20. Liu ZH, Yang ZZ, Yu XX, Zhang HY, Yu B, Zhao YF, Liu ZM (2017) Methylation of $C(sp^3)$-H/$C(sp^2)$-H bonds with methanol catalyzed by cobalt system. Org Lett 19:5228–5231. https://doi.org/10.1021/acs.orglett.7b02462
21. Campanati M, Savini P, Tagliani A, Vaccari A (1997) Environmentally friendly vapour phase synthesis of alkylquinolines. Catal Lett 47:247–250. https://doi.org/10.1023/A:1019033811243
22. Hu Y, Lü WH, Liu DY, Shi L, Sun Q (2009) Effect of ZnO on the performance of Ag/SiO_2 catalyst for the vapor-phase synthesis of 3-methylindole. J Nat Gas Catal 18:445–448. https://doi.org/10.1016/S1003-9953(08)60139-5
23. Gopal DV, Srinivas B, Durgakumari D, Subrahmanyam M (2002) Vaper-phase alkylation of indole with methanol over zeolites. J Appl Catal 224:121–128. https://doi.org/10.1016/S0926-860X(01)00787-6
24. Lü WH, Liu XH, Liu DY, Shi L, Sun Q (2009) Vapor-phase synthesis of 3-methylindole over Fe-, Co-, or Ni-promoted Ag/SiO_2 catalysts. Chin J Catal 30:1287–1290. https://doi.org/10.1016/S1872-2067(08)60145-X
25. Simoneau CA, Strohl AM, Ganem B (2007) One-pot synthesis of polysubstituted indoles from aliphatic nitro compounds under mild conditions. Tetrahedron Lett 48:1809–1811. https://doi.org/10.1016/j.tetlet.2007.01.031
26. Choi I, Chung H, Park JW, Chung YK (2016) Active and recyclable catalytic synthesis of indoles by reductive cyclization of 2-(2-nitroaryl)acetonitriles in the presence of Co-Rh heterobimetallic nanoparticles with atmospheric hydrogen under mild conditions. Org Lett 18:5508–5511. https://doi.org/10.1021/acs.orglett.6b02659
27. Kanchupalli V, Joseph D, Katukojvala S (2015) Pyridazine N-oxides as precursors of metallocarbenes: rhodium-catalyzed transannulation with pyrroles. Org Lett 17:5878–5881. https://doi.org/10.1021/acs.orglett.5b03064
28. Zhou CH, Zhao H, Tong DS, Wu LM, Yu WH (2013) Recent advances in catalytic conversion of glycerol. Catal Rev Sci Eng 55:369–453. https://doi.org/10.1080/01614940.2013.816610
29. Wang ZY, Li XH, Zhang Y, Shi L, Sun Q (2012) Effect of alkaline-earth metal oxides on Cu/SiO_2-Al_2O_3 catalyst for vapor-phase synthesis of 3-methylindole from glycerol and aniline. Chinese J Catal 33:1139–1145. https://doi.org/10.1016/S1872-2067(11)60407-5
30. Cui YX, Zhou XS, Sun Q, Shi L (2013) Vapor-phase synthesis of 3-methylindole from glycerol and aniline over

zeolites-supported Cu-based catalysts. J Mol Catal A Chem 378:238–245. https://doi.org/10.1016/j.molcata.2013.06.015
31. Ke KX, Wu FL, Ren LT, Jiao YB, Xing N, Shi L (2019) An efficient catalyst of Cu/MIL-101 modified with CeO_2 for the conversion of biomass-derived glycerol with aniline to 3-methylindole. Catal Commun. https://doi.org/10.1016/j.catcom.2019.105896
32. Zhao JB, Yuan HF, Qin XM, Tian K, Liu YF, Wei CZ, Zhang ZQ, Zhou LM (2020) Au nanoparticles confned in SBA-15 as a highly efficient and stable catalyst for hydrogenation of quinoline to 1,2,3,4-tetrahydroquinoline. Catal Lett. https://doi.org/10.1007/s10562-020-03190-3
33. Nouri K, Hajjami M, Azadi G (2018) Pd-4,6-diamino-2-pyrimidinethiol complex supported on SBA-15 as a useful and retrievable catalyst for suzuki-miyaura and stille C-C coupling reactions. Catal Lett 148(2):671–679. https://doi.org/10.1007/s10562-017-2290-3
34. Yu S, Cao X, Li L, Liu S, Wu Q (2018) Catalytic cracking of rubber seed oil using basic mesoporous molecular sieves K_2O/MeO-SBA-15 (Me = Ca, Mg or Ba) as heterogeneous catalysts for the production of liquid hydrocarbon fuels. Catal Lett 148:3787–3796. https://doi.org/10.1007/s10562-018-2555-5
35. Elías VR, Benzaquén TB, Rodríguez PAO, Cuello NI, Tolley A, Eimer GA (2020) Elucidating iron speciation tuned by handling metal precursor for more efficient designing of nanostructured Fenton catalysts. Catal Lett 150(5):196–208. https://doi.org/10.1007/s10562-019-02921-5
36. Albuquerque JS, Costa FO, Barbosa BVS (2019) Fischer-Tropsch synthesis: analysis of products by Anderson-Schulz-Flory distribution using promoted cobalt catalyst. Catal Lett. https://doi.org/10.1007/s10562-019-02655-4
37. Restrepo-Garcia JR, Ramírez GE, Baldovino-Medrano VG (2017) Hydroprocessing of phenanthrene over sulfided Fe–W supported on modified SBA-15. Catal Lett 148(2):621–641. https://doi.org/10.1007/s10562-017-2269-0
38. Palai YN, Anjali K, Sakthivel A, Ahmed M, Sharma D, Badamali SK (2017) Cerium ions grafted on functionalized mesoporous SBA-15 molecular sieves: preparation and its catalytic activity on p-cresol oxidation. Catal Lett 148(1):465–473. https://doi.org/10.1007/s10562-017-2238-7
39. Zhao D, Huo Q, Feng J, Chmelka BF, Stucky GD (1998) Nonionic triblock and star diblock copolymer and oligomeric surfactant syntheses of highly ordered, hydrothermally stable, mesoporous silica structures. J Am Chem Soc 120:6024–6036. https://doi.org/10.1021/ja506344k
40. Anjali K, Ahmed M, Christopher J, Sakthivel A (2018) Rhodium-calix[4]pyrrole and rhodium-tetraphenyl porphyrin: preparation, surface grafting and their catalytic application in nitro-benzene reduction. Dalton Trans. https://doi.org/10.1039/c8dt02151a
41. Mohammadi Ziarani G, Rohani S, Ziarati A, Badiei A (2018) Applications of SBA-15 supported Pd metal catalysts as nanoreactors in C-C coupling reactions. RSC Adv 8(71):41048–41100. https://doi.org/10.1039/c8ra09038f
42. Andrei RD, Cambruzzi N, Bonne M, Lebeau B, Hulea V (2018) Selective sulfoxidation reactions with H_2O_2 catalyzed by Ti-containing SBA-15 materials. J Porous Mater 26:533–539. https://doi.org/10.1007/s10934-018-0640-1
43. Jin MM, Niu QT, Si CD, Lv ZG, Guo HY, Guo ZM (2019) Peroxotungstate-based ionic hybrid as a triphase heterogeneous catalyst for efficient benzyl alcohol oxidation under mild conditions. Catal Lett. https://doi.org/10.1007/s10562-019-03071-4
44. Yadav R, Muralidhar A, Shamna A, Aghila P, Gurrala L, Sakthivel A (2018) Aluminium oxide supported on SBA-15 molecular sieves as potential Lewis acid catalysts for epoxide ring opening using aniline. Catal Lett 148(5):1407–1415. https://doi.org/10.1007/s10562-018-2366-8
45. Khatun R, Bhanja P, Molla RA, Ghosh S, Bhaumik A, SkM I (2017) Functionalized SBA-15 material with grafted CO_2H group as an efficient heterogeneous acid catalyst for the fixation of CO_2 on epoxides under atmospheric pressure. Mol Catal 434:25–31. https://doi.org/10.1016/j.mcat.2017.01.013
46. Derylo-Marczewska A, Marczewski AW, Skrzypek I, Pikus S, Kozak M (2008) Effect of addition of pore expanding agent on changes of structure characteristics of ordered mesoporous silicas. Appl Surf Sci 255:2851–2858. https://doi.org/10.1016/j.apsusc.2008.08.026
47. Vargas-Hernándeza D, Rubio-Caballerob JM, Santamaría-Gonzálezb J, Moreno-Tost R, Mérida-Robles JM, Pérez-Cruz MA, Jiménez-López A, Hernández-Huesca R, Maireles- Torres P (2014) Furfuryl alcohol from furfural hydrogenation over copper supported on SBA-15 silica catalysts. J Mol Catal A 34:106–113. https://doi.org/10.1016/j.molcata.2013.11.034
48. Gao SS, Xu ST, Wei YX, Qiao QL, Xu ZC, Wu XQ, Zhang MZ, He YL, Xu SL, Liu ZM (2018) Insight into the deactivation mode of methanol-to-olefins conversion over SAPO-34: coke, diffusion, and acidic site accessibility. J Catal 367:306–314. https://doi.org/10.1016/j.jcat.2018.09.010
49. Cai FF, Jin FK, Hao J, Xiao GM (2019) Selective hydrogenolysis of glycerol to 1,2-propanediol on Nb-modified Pd-Zr-Al catalysts. Catal Commun 131:105801. https://doi.org/10.1016/j.catcom.2019.105801
50. Kinage AK, Upare PP, Kasinathan P, Hwang YK, Chang JS (2010) Selective conversion of glycerol to acetol over sodium-doped metal oxide catalysts. Catal Commun 11:620–623. https://doi.org/10.1016/j.catcom.2010.01.008
51. Gabrysch T, Muhler M, Peng B (2019) The kinetics of glycerol hydrodeoxygenation to 1,2-propanediol over Cu/ZrO_2 in the aqueous phase. Appl Catal A 576:47–53. https://doi.org/10.1016/j.apcata.2019.03.001
52. Zhou CH, Deng K, Serio MD, Xiao S, Tong DS, Li L, Lin CX, Beltramini J, Zhang H, Yu WH (2017) Cleaner hydrothermal hydrogenolysis of glycerol to 1,2-propanediol over Cu/oxide catalysts without addition of external hydrogen. Mol Catal 432:274–284. https://doi.org/10.1016/j.mcat.2017.02.008
53. Miyazawa T, Koso S, Kunimori K, Tomishige K (2007) Glycerol hydrogenolysis to 1,2-propanediol catalyzed by a heat-resistant ion-exchange resin combined with Ru/C. Appl Catal A 329:30–35. https://doi.org/10.1016/j.apcata.2007.06.019
54. Montes V, Checa M, Marinas A, Boutonnet M, Marinas JM, Urbano FJ, Järas S, Pinel C (2014) Synthesis of different ZnO-supported metal systems through microemulsion technique and application to catalytic transformation of glycerol to acetol and 1,2-propanediol. Catal Today 223:129–137. https://doi.org/10.1016/j.cattod.2013.09.021
55. Zheng JC, Liu J, Tan W, Shi L, Sun Q (2008) Vapor phase synthesis of 3-methylindole over a Ag/SiO_2 catalyst. Chin J Catal 29:1199–1201. https://doi.org/10.1016/S1872-2067(09)60025-5